crystals

MDPI

Review

Organic Nonlinear Optical Crystals for Highly Efficient Terahertz-Wave Generation

Ying Yang, Xinyuan Zhang *, Zhanggui Hu [1] and Yicheng Wu

Tianjin Key Laboratory of Functional Crystal Materials, Institute of Functional Crystals, Tianjin University of Technology, Tianjin 300384, China

* Correspondence: xyzhang@email.tjut.edu.cn

Abstract: Terahertz (THz) technology is an emerging field that is promising for future applications. Nonlinear optical (NLO) materials can effectively convert incident light into the THz frequency range using optics methods. Ionic-type organic π-conjugated NLO crystals containing electron donor-π-acceptor motifs have long attracted attention for their possibility to achieve large nonlinear optical coefficients. In this paper, an overview of the recent progress in ionic-type organic NLO crystals for highly efficient THz wave generation is presented. The substitution design strategies of cations and anions, for increasing optical nonlinearities and reducing absorptions in different structure series, are summarized. In addition, the progress in crystal growth and their THz output performance are also discussed.

Keywords: π-conjugated nonlinear optical (NLO) crystals; crystal growth; THz output

check for updates

Citation: Yang, Y.; Zhang, X.; Hu, Z.; Wu, Y. Organic Nonlinear Optical Crystals for Highly Efficient Terahertz-Wave Generation. *Crystals* **2023**, *13*, 144. https://doi.org/10.3390/cryst13010144

Academic Editor: Yuri Kivshar

Received: 16 December 2022
Revised: 3 January 2023
Accepted: 8 January 2023
Published: 13 January 2023

Copyright: © 2023 by the authors. Licensee MDPI, Basel, Switzerland. This article is an open access article distributed under the terms and conditions of the Creative Commons Attribution (CC BY) license (https://creativecommons.org/licenses/by/4.0/).

1. Introduction

Organic nonlinear optical (NLO) crystals have attracted increasing attention for their promising applications in terahertz (THz) photonics, such as electromagnetic waves, THz generation, and detection [1–5]. Compared with inorganic crystals (e.g., $ZnGeP_2$, $LiNbO_3$, GaSe, etc.), organic NLO crystals generally show good optical nonlinearity, an ultrafast response time, as well as various design possibilities [6–15].

Ionic-type organic NLO crystals are constructed from cations and anions that are different from molecular-type NLO crystals, and it is known that cations are the main source of the nonlinearities [16–18]. In this kind of crystal structure, the D-π-A structure is the basic framework of the cation, which is composed of the electron donor (D) part and an electron acceptor (A) part, connected via a π-conjugated bridge. Based on the D-π-A structure, molecules can exhibit large first-order hyperpolarizabilities, which are beneficial for obtaining large macroscopic nonlinear optical susceptibilities, when the molecules crystallize in non-centrosymmetric space groups. Although the contribution of anions to the microscopic first-order hyperpolarization is negligible, different anions can regulate the stacking form of cationic chromophores in the crystal, as well as induce a non-centrosymmetric arrangement [19]. Typical anions include alkyl-substituted benzenesulfonate anions (e.g., T, TMS) and halogenated substituted benzenesulfonate anions (e.g., CBS, BBS). DAST (Supplementary Materials) is one of the most famous crystals and contains a T anion with a great nonlinear optical coefficient (d_{11} = 210 ± 55 pm/V) at 1.9 μm fundamental frequency light [20]. However, inherent defects, such as an easy deliquescence, strong absorption near 1 THz, and poor mechanical properties, have for a long time limited the further practical application of DAST as a commercial optical device.

Based on the excellent properties of DAST, a series of derivatives of DAST have also been developed by introducing different counter anions [21–26]. To explore this kind of ionic-type organic nonlinear optical crystal for THz generators with improved properties, the following points are usually considered: (i) large macroscopic second-order optical nonlinearity; (ii) good phase matching between light waves and terahertz waves; (iii) reducing

self-absorption in the THz region; and (iv) stable physical and chemical properties [27,28]. In recent years, researchers have found that the combination of strong electron donors and acceptors, which can produce strong hydrogen bonds between electronegative groups and the molecular skeleton, is very beneficial for suppressing the THz absorption modes of organic electro-optic salt crystals [27,29]. Through this strategy, the contribution of π-π stacking interactions and hydrogen bonds to the secondary bond interactions can be controlled, not only achieving the purpose of restraining the molecular vibration mode in the crystalline state, but also obtaining a favorable spatial arrangement [29].

In this review, we summarize the selection of cations and anions in different ionic-type NLO crystal series that have been proven THz generation in recent five years. The effects of different substitution groups on macroscopic optical nonlinearity and physicochemical properties are discussed. Moreover, the progress in crystal growth and THz output applications is also briefly summarized.

2. Discussion

2.1. Pyridinium-Based THz Crystals

Benchmark DAST ($C_{23}H_{26}N_2O_3S$, *Cc*) has an extremely large nonlinear optical coefficient d_{11} = 210 ± 55 pm/V at 1.9 μm [20]. The DAS cation (Figure 1) with strong -N(CH_3)$_2$ donor group exhibits a large maximum first-order hyperpolarization, i.e., β_{max} = 159 × 10^{-30} esu, corresponding to the maximum absorption wavelength (λ_{max}) of 475 nm in methanol solution [30]. However, the obvious absorption peak of DAST crystal in the terahertz-wave region (~1 THz), centrosymmetric hydrate, and difficulties in crystal growth have long hindered progress in its practical use [31,32]. The discovery of DAST opens up new horizons for terahertz-wave sources and recent work has made much efforts in the development of novel crystals with improved properties.

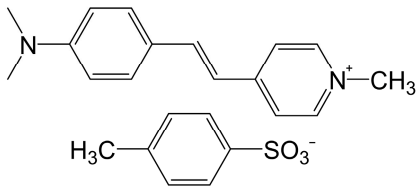

Figure 1. Chemical structure of DAST.

Hydroxyl (-OH), as a classical electron donor, shows a high tendency to form a non-Coulomb interionic assembly with benzenesulfonate anions, which can contribute more hydrogen bonds to the crystalline states. Newly developed pyridinium derivatives with phenol groups, e.g., OHP and DHP cations (Figure 2 and Table 1), have provided excellent properties through two push-pull-type aromatic rings with one or two hydroxyl groups [28,33]. Based on quantum chemical calculations with density functional theory (DFT) [34], the OHP cation exhibits large microscopic optical nonlinearity with a non-resonant maximum first-order hyperpolarizability β_{max} of 125 × 10^{-30} esu, corresponding to the maximum absorption wavelength (λ_{max}) of 392 nm in methanol (10^{-3} M) (OHP-TFS). Through quantum chemical calculation with the DFT at the B3LYP/6-311+G (d, p) level, the average value of β_{max} in the optimized DHP cation with two phenolic -OH groups is 121 × 10^{-30} esu and the maximum absorption wavelength (λ_{max}) of DHP-TFS is approximately 406 nm in methanol. Compared with DAST (475 nm in methanol), the maximum absorption wavelengths of OHP-TFS and DHP-TFS are blue-shifted by 83 nm and 69 nm, respectively. These two pyridinium-based crystals with phenol groups exhibit a yellow color, probably indicating enlarged bandgaps and a broadened pump wavelength region.

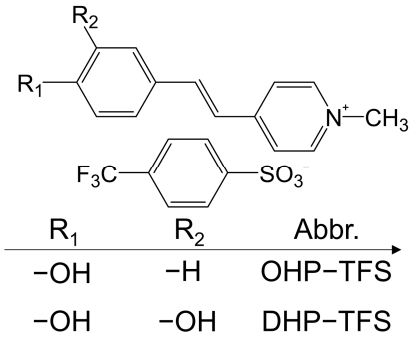

Figure 2. Chemical structures of pyridinium-based OHP-TFS and DHP-TFS.

In order to reduce the vibrational amplitude in the crystal, the TFS anion with strongly electronegative -CF_3 is introduced to increase the interaction and reduce the void volume (or increase the density), which can form strong hydrogen bonding interactions between phenolic groups on cations [27]. In OHP-TFS crystal, the OHP cations are perfectly aligned in parallel, as shown as Figure 3a,b, which leads to maximizing the value of the diagonal effective hyperpolarizability tensor to a level equivalent to that of DAST, indicating that OHP-TFS would also exhibit a strong SHG intensity [28]. As shown in Figure 3c, the catechol group causes DHP cations and TFS anions to form two strong hydrogen bonds, with distances of 1.86 Å and 2.14 Å, respectively. The DHP-TFS crystal exhibits a parallel-type cation-anion assembly (Figure 3d), which is similar to the classic DAST, and the average value of $(I_{DHP\text{-}TFS}/I_{DAST})^{0.5}$ is ≈ 0.7 under the fundamental light ≥1500 nm [33].

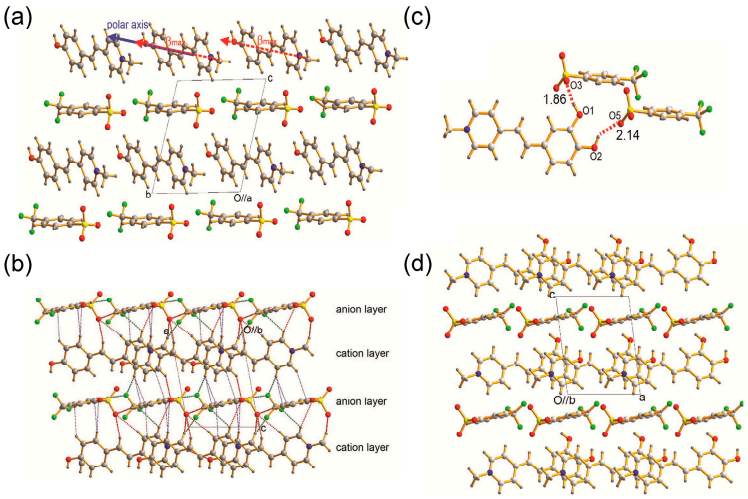

Figure 3. (**a**) The OHP chromophores are perfectly aligned in parallel along the *a*-axis, and (**b**) 3D network-like interionic interactions between cation layers and anion layers in OHP-TFS [28]; (**c**) catechol induced strong hydrogen bonds between DHP cations and TFS anions, and (**d**) molecular alignment of DHP-TFS crystals [33].

Table 1. Comparison of the mentioned pyridinium-based THz crystals.

Crystal Name	Space Group	λ_{max}(nm) in Methanol	β_{max} (Cation)	SHG Intensity	Ref.
DAST	Monoclinic *Cc*	475	159×10^{-30} esu	$d_{11} = 210 \pm 55$ pm/V at 1.9 μm	[20]
OHP-TFS	Triclinic *P*1	392	125×10^{-30} esu	~DAST	[28]
DHP-TFS	Triclinic *P*1	406	121×10^{-30} esu	~0.49 × DAST, ≥1500 nm	[33]

2.2. Quinolinium-Based THz Crystals

Quinolinium is one of the strong acceptors [35–37]. In the last five years, various quinolinium-based NLO crystals have been developed. Generally, quinolinium-based cations include two types, namely, halogen-free and halogen-containing quinolinium-based electron acceptors.

2.2.1. Halogen-Free Cations

HMQ is a classical cation with two strong electron donors (-OH and -OCH_3), which was first reported as an efficient cation of THz crystal in 2012 [38]. This HMQ cation exhibits a larger first-order hyperpolarization, β_{max} = 145 × 10^{-30} esu, than that of the OH1 molecule (104 × 10^{-30} esu), and the maximum absorption λ_{max} (439 nm) of the HMQ cation is also larger than OH1 (426 nm) [39]. More recently, quinolinium-based cations have been designed by learning from the structure of HMQ (Figure 4 and Table 2). Another successful cation is OHQ with only one -OH substitution, which was first reported in 2015 [40]. By using quantum chemical calculation based on finite field DFT using B3LYP/6-311+G*, OHQ retains a relatively small hyperpolarizability along the main charge-transfer direction (118 × 10^{-30} esu), and the maximum absorption wavelength of OHQ-based crystal (425 nm) is blue-shifted by 14 nm compared with HMQ-based crystals (439 nm) in methanol.

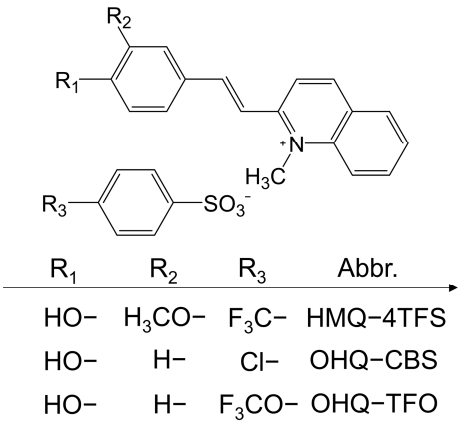

Figure 4. Chemical structures of quinolinium-based compounds with a halogen-free cation.

2.2.2. Halogen-Containing Cations

To further enlarge the microscopic nonlinearity, halogen substitutions are selected for quinolinium-based electron acceptors, as shown in Figure 5 and Table 2. There are different substitution sites on the quinolinium ring. Through halogen substitution, σ-hole engineering can be applied to organic crystals [41]. Through the introduction of the -Cl group into the quinolinium-based electron acceptor cations, the HM7ClQ cation with increased first-order hyperpolarization was obtained [42]. The maximal first-order hyperpolarizability β_{max} of HM7ClQ-based cations is ~170 × 10^{-30} esu, and the maximum absorption wavelength of HM7ClQ chromophore is 450 nm in methanol, which is red-shifted compared with nonhalogenated HMQ (Figure 4) chromophore (439 nm). However, unlike other halogen groups (e.g., -Cl, -Br, and -I), the -F group cannot produce σ-holes in this cation series. Through finite field (FF) quantum chemical calculation at B3LYP/6-311+G(d) level, the first hyperpolarizability β_{max} of HM6FQ only amounts to 140 × 10^{-30} esu, which is very similar to that of the nonfluorinated HMQ cation (145 × 10^{-30} esu), and the maximum absorption wavelength of the HM6FQ (444 nm) cation is almost the same as nonfluorinated HMQ cations (439 nm) in methanol [43].

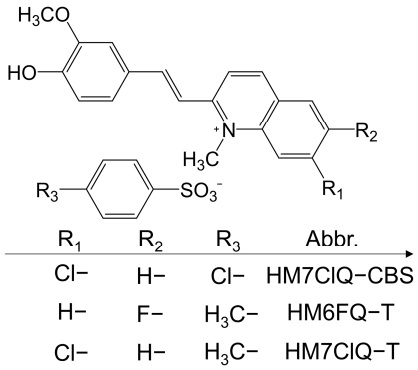

Figure 5. Chemical structures of quinolinium-based HM7ClQ-CBS, HM6FQ-T, and HM7ClQ-T.

2.2.3. Effects of Halogen-Containing Anions on the Spatial Arrangement

Under the control of the TFS anion, the first hyperpolarizabilities of the HMQ cation in HMQ-4TFS crystals and the polar axis of the crystal are almost in the same direction; namely, the molecular-ordering angle is close to zero, as shown in Figure 6a [29]. The π-π stacking distance of HMQ cations in HMQ-4TFS is 3.62 Å, which is longer than HMQ-T, indicating an attenuation of the strength of π-π interactions. With the help of the 4TFS anion, the SHG intensity of HMQ-4TFS is proven comparable to DAST under the fundamental wavelength of 1250 nm. As shown in Figure 6b, OHQ cations are perfectly arranged in parallel with the help of CBS anions, and the molecular order angle is zero. In OHQ-CBS crystal, the cation layers and anion layers are connected by hydrogen bonds with a distance of 1.82 Å, and the SHG intensity of OHQ-CBS is about 1.2 times that of DAST at 1500 nm [44]. In OHQ-TFO crystal, the ordering angle θ_p between the polar axis and the direction of the maximal first-order hyperpolarizability β_{max} is rather small (θ_p = 12.1°) (Figure 6c) [45]. In OHQ-TFO, the non-planar shaped -OCF_3 can produce a large steric hindrance, as well as reduce the π electron density of aryl atoms on anions, preventing edge-to-face π-π cation–anion interactions and leading to an enhanced macroscopic optical nonlinearity (SHG ~2.3 × DAST at 1150 nm). As shown in Figure 6d, HM7ClQ cations are arranged head-to-tail in the same direction with the help of CBS anions. HM7ClQ-CBS crystal with both anions and cations chlorinated exhibits a large SHG intensity, about 1.2 times that of a DAST crystal at wavelength >1400 nm [42].

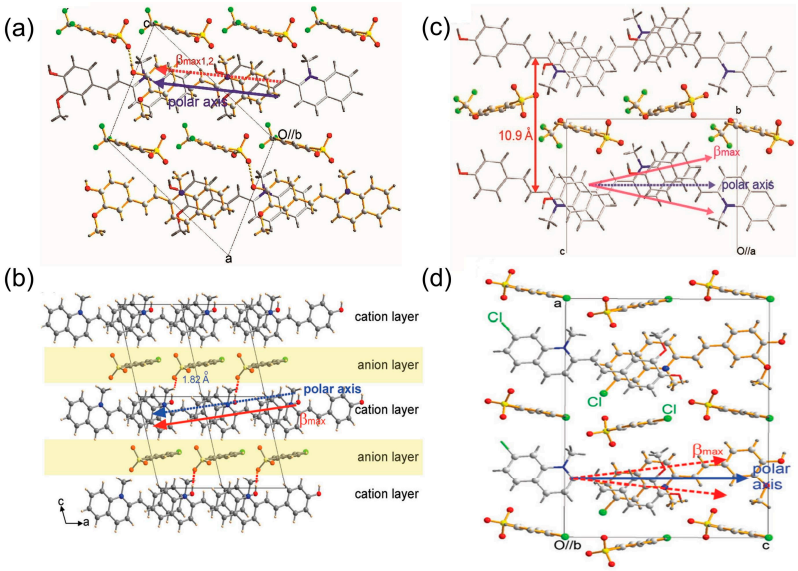

Figure 6. (**a**) Molecular packing diagram of HMQ-4TFS [29] and (**b**) OHQ-CBS crystals projected along the crystallographic *b*-axis [44]; (**c**) molecular packing diagram of OHQ-TFO crystal projected along the crystallographic *a*-axis [45]; and (**d**) molecular packing diagram of HM7ClQ-CBS crystal along the *a*-axis [42].

2.2.4. Effects of Halogen-Free Anions on the Spatial Arrangement

The T anion group is one of the classical anions, not only in pyridium-based DAST, but also in quinolinium-based compounds. With the help of T anions, the earliest classical HMQ and OHQ chromophores can be induced in asymmetrically crystal space groups, with the SHG intensity separately reaching 0.63 and ~1 times that of DAST under 1.9 μm and 1245 nm fundamental light [38,40]. Due to this, T anions are also introduced in combination with newly designed halogen-containing cations. The molecular arrangement of the recently developed HM6FQ-T crystal with the classical T anion is shown in Figure 7a, in which the hydrogen bond distances induced by -F substitutions are <3 Å (2.16 Å for F ··· H on anionic benzene ring carbon, 2.80 Å for F ··· H on anionic methyl carbon, and 2.83 Å for F ··· H on anionic benzene ring carbon). The molecular-ordering angle θ_p of HM6FQ-T is 15.3°, showing a large SHG intensity of about 0.63 times DAST at 1150–1900 nm. Under the action of the anion T, HM7ClQ cations are connected head-to-tail in the same direction, as shown in Figure 7b. The molecular ordering angle θ_p between the direction of the first hyperpolarizability β_{max} and the polar axis of HM7ClQ-T crystals is very small (θ_p = 8.2°), and the corresponding order parameter is $\cos^3\theta_p$ = 0.97, which is close to the maximum value $\cos^3\theta_p$ = 1, while the SHG intensity is comparable to DAST at >1400 nm.

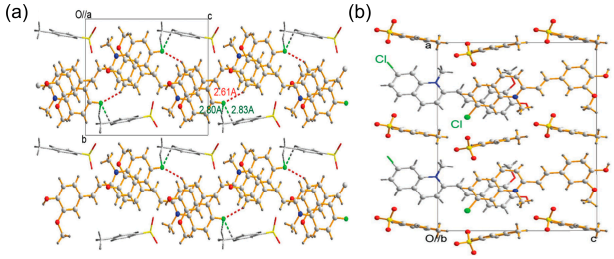

Figure 7. (**a**) Packing diagram of HM6FQ-T [43] crystal along the crystallographic *a*-axis and (**b**) arrangement of HM7ClQ-T along the *b*-axis [42].

Table 2. Comparison of the mentioned quinolinium-based THz crystals.

Crystal Name	Space Group	λ_{max}(nm) in Methanol	β_{max} (Cation)	SHG Intensity	Ref.
HMQ-4TFS	Monoclinic *Pn*	439	145 × 10^{-30} esu	~DAST at 1250nm	[29]
OHQ-CBS	Triclinic *P*1	425	~118 × 10^{-30} esu	1.2 × DAST at 1500 nm	[44]
OHQ-TFO	Monoclinic *Pc*	425	~118 × 10^{-30} esu	~2.3 × DAST at 1150 nm	[45]
HM7ClQ-CBS	Orthorhombic *Pna*2_1	450	~170 × 10^{-30} esu	~1.2 × DAST at >1400 nm	[42]
HM6FQ-T	Monoclinic *Pn*	444	140 × 10^{-30} esu	0.63 × DAST at 1150–1900 nm	[43]
HM7ClQ-T	Orthorhombic *Pna*2_1	450	~170 × 10^{-30} esu	~DAST at >1400 nm	[42]

2.3. Benzothiazolium-Based THz Crystals

2.3.1. Halogen-Free Cations

The benzothiazolium-based cations with large first-order hyperpolarizability mainly include PMB, HMB, and HDB cations (Figure 8, Table 3) [46–48]. PMB cation consists of a strong electron-donating dialkylamino group, and the calculated first-order hyperpolarizability of the PMB cation is about 274 × 10^{-30} esu, which is much larger than that of DAST crystal (159 × 10^{-30} esu). Correspondingly, the maximum absorption wavelength of the PMB cation is 523 nm, presenting a redshift of 48 nm compared with DAST (475 nm). Combined with classical electron donor -OH and -CH_3/OCH_3, the HMB cation and HDB cation show large maximum absorption wavelengths of 438 nm and 566 nm in methanol. In addition, the OHB cation in OHB-TFO only contains one hydroxyl donor, showing a not very large first-order hyperpolarizability of 100 ± 7 × 10^{-30} esu, while the maximum absorption wavelength in methanol solution is 419 nm [49].

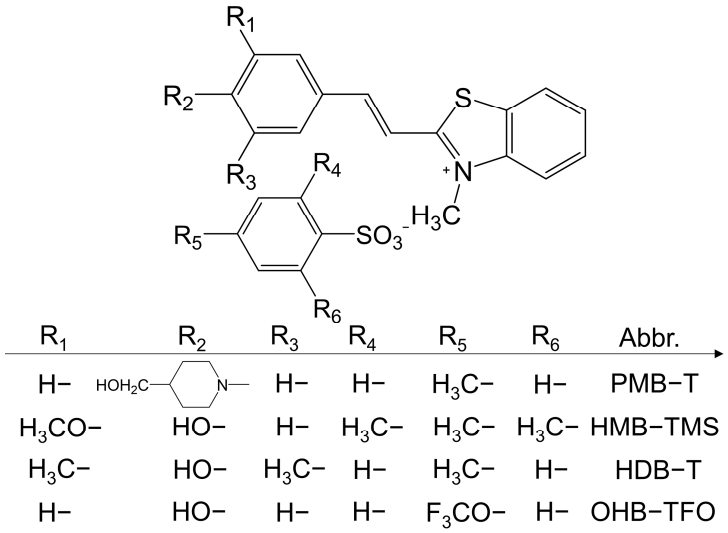

Figure 8. Chemical structures of benzothiazolium-based NLO crystals.

2.3.2. Halogen-Containing Cations

The maximum absorption wavelength of PFB (Figure 9, Table 3) chromophore in methanol is 533 nm, which is slightly higher than that of nonfluorinated benzothiazolium-based chromophore PMB (523 nm) [50].

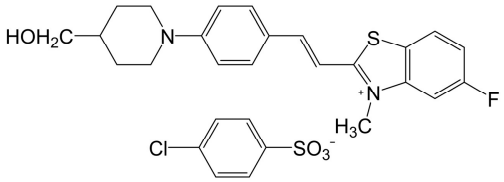

Figure 9. Chemical structure of benzothiazolium-based PFB-CBS.

2.3.3. Effects of Halogen-Free Anions on the Spatial Arrangement

PMB-T crystal can form series-type cation-anion assembly through strong bidentate-like hydrogen bonds between the PMB cationic terminal HO- group and the sulfonate on T anions (Figure 10a,b) [46]. At the reference wavelength of 1800 nm, PMB-T exhibits a large SHG intensity comparable to DAST. The strongest hydrogen bonds were formed between the phenolic hydroxyl group on the cations and the sulfonate group on the anions (–O–H $\cdots^{-}$ OS–), with a distance of 1.902 Å (Figure 10c) for HMB-TMS [47]. The molecular order angle of the HMB-TMS crystal is close to zero, showing a large SHG intensity similar to that of DAST at 1250 nm. Two kinds of strong hydrogen bonds are formed between the phenolic group (-OH) of the HDB-T cation and the sulfonate group ($-SO_3^-$) on the anion (Figure 10d). The hydrogen bond distances between H atoms in hydroxyl groups and O atoms in sulfonic groups are 1.884 and 2.044 Å for the two different oriented HDB cations, respectively. HDB cations stack with each other at an angle of 16.46° through face-to-face π-π stacking interactions, and each layer is in the same direction at an angle of 66.91° along the *c*-axis in HDB-T (Figure 10d) and with an X-shaped arrangement. In this way, the microscopic nonlinearity can be effectively accumulated, and the SHG intensity of HDB-T reaches 1.5 times that of OH1 at 2090 nm [48].

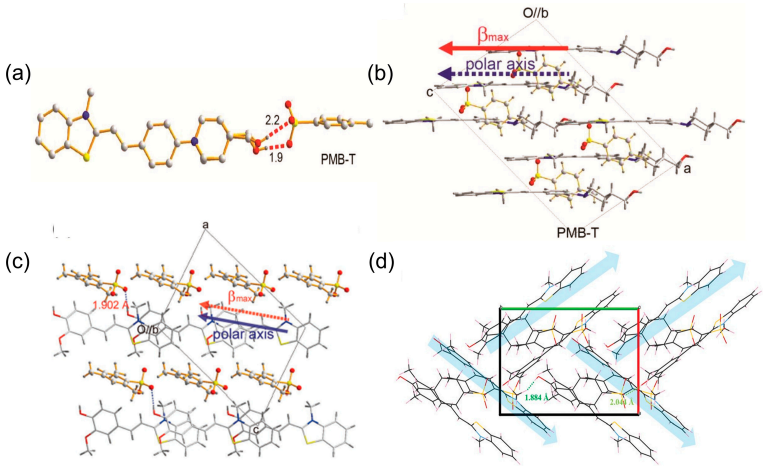

Figure 10. (**a**) Interaction between the anion and cation of PMB-T; (**b**) packing of PMB-T along the *b*-axis [46]; (**c**) packing of HMB-TMS along the *b*-axis [47]; and (**d**) crystal packing diagram of HDB-T crystal [48].

2.3.4. Effects of Halogen-Containing Anions on the Spatial Arrangement

The chemical structures of PMB-based crystals are shown in Figure 11a. In PMB-4TFS crystal, there are double hydrogen bond donors at both ends of the PMB cations and double hydrogen bond receptors at both ends of TFS anions [27]. Anions and cations can be connected head-to-tail, to form a large number of hydrogen bond interactions, i.e., Ar-H (cation) … F (anion)-SO_3^- (anion) … H-O (cation), as shown in Figure 11b. Regarding the TFO anion, the molecular order angle for PMB-TFO is 56°, leading to a V-shaped arrangement (Figure 11c) [51]. The SHG signal of PMB-TFO is comparable to that of DAST under a wavelength of ≥1400 nm. As shown in Figure 11d, under the regulation of CBS anions, the cations in the PFB-CBS crystal structure are also cross-arranged in the same direction (X-shaped arrangement) and the SHG intensity ratio $(\eta/\eta_{DAST})^{0.5}$ is 0.82 [50].

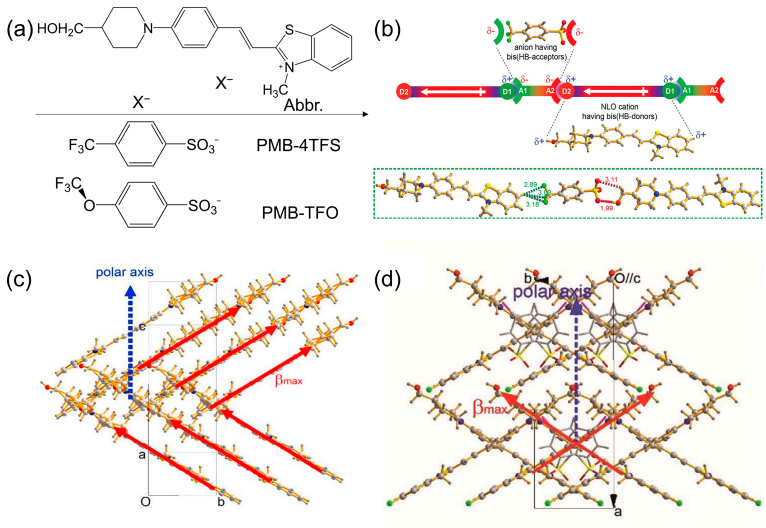

Figure 11. (**a**) Chemical structures of benzothiazolium-based NLO crystals; (**b**) PMB-4TFS double head-to-tail hydrogen bond assembly [27]; (**c**) arrangement of PMB cations in PMB-TFO [51]; and (**d**) arrangement of PFB-CBS crystals along the *c*-axis [50].

Table 3. Comparison of the mentioned benzothiazolium-based THz crystals.

Crystal Name	Space Group	λ_{max}(nm) in Methanol	β_{max} (Cation)	SHG Intensity	Ref.
PMB-T	Monoclinic *Cc*	523	274×10^{-30} esu	~DAST at 1800 nm	[46]
HMB-TMS	Monoclinic *Pn* (m)	438	$>162 \times 10^{-30}$ esu	~DAST at 1250 nm	[47]
HDB-T	Monoclinic $P2_1$	566	-	1.5 × OH1 at 2090 nm	[48]
OHB-TFO	Monoclinic *Cc*	419	$100 \pm 7 \times 10^{-30}$ esu	0.3 × DAST at 1500 nm	[49]
PFB-CBS	Monoclinic *Cc*	533	$\sim 274 \times 10^{-30}$ esu	~0.67 × DAST at 1800 nm	[50]
PMB-4TFS	Monoclinic *Cc*	523	274×10^{-30} esu	-	[27]
PMB-TFO	Monoclinic *Cc*	523	274×10^{-30} esu	~DAST at ≥1400 nm	[51]

2.4. Indolium-Based THz Crystals

2.4.1. Classical Cations

As shown in Figure 12 and Table 4, EHPSI-4NBS was designed with hydroxypiperidine as a strong electron donor, and the calculated β_{max} amounts to 123×10^{-30} esu, corresponding to a maximum absorption wavelength of 549 nm in methanol [52]. Another indolium-based NLO crystal, OHI-T (Figure 12), also contains hydroxyl as an electron donor, and the maximum absorption wavelength of the OHI cation in methanol is 437 nm, which is slightly larger than OH1 (λ_{max} = 426 nm) and quinolinium-based OHQ (λ_{max} = 425 nm) (Figure 4) [53].

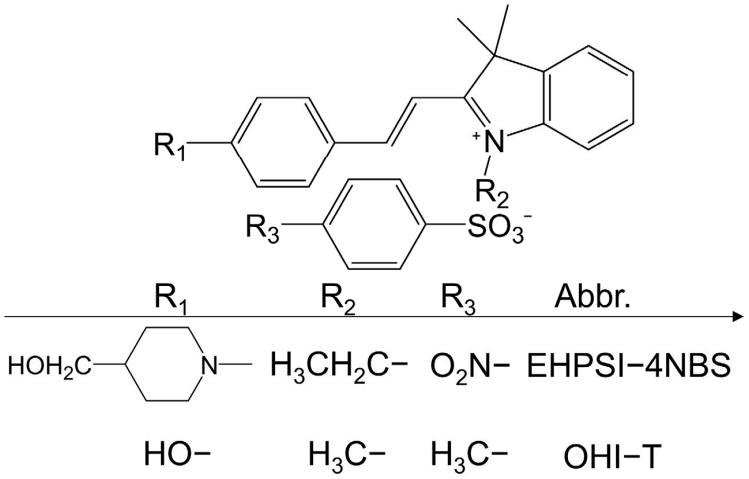

Figure 12. Chemical structures of indolium-based EHPSI-4NBS and OHI-T.

2.4.2. Effect of Anions on the Spatial Arrangement

With the help of the NBS anion, the molecular order angle of EHPSI-4NBS is 2.5°, which represents the chromophore being perfectly arranged in parallel (Figure 13a). The introduction of the T anion induces the OHI cations to arrange in the same direction and effectively accumulate the microscopic first-order hyperpolarization via strong hydrogen bonds (1.787 Å) (Figure 13b). Therefore, this nearly perfect cation arrangement leads to a strong macroscopic second-order nonlinear response of OHI-T ~0.7 × OH1 at 2.09 μm. OHI-T has a wide transmission range from 504 nm to 2100 nm with a large bandgap (2.47 eV) [53].

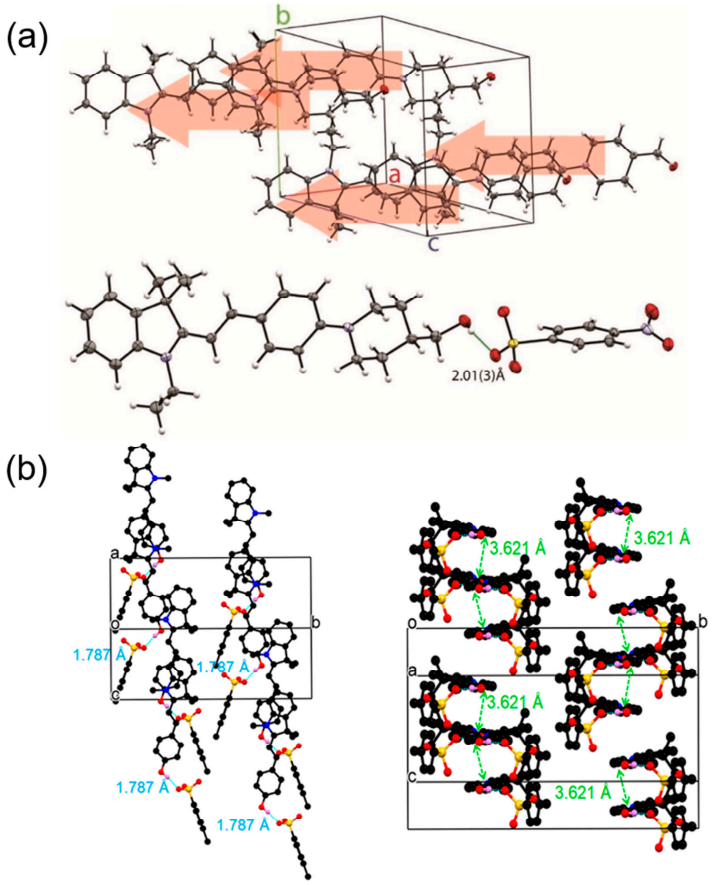

Figure 13. (**a**) Crystal stacking of EHPSI-4NBS [52], and (**b**) molecular stacking along the [101] direction in OHI-T [53].

2.5. Benzoindolium-Based THz Crystals

2.5.1. Cations with Classical Electron Donor

P-BI is the only benzoindolium-based NLO crystal that has been proven with terahertz-wave generation in the recent five years, and there is an obvious absorption peak around 2 THz [54]. Considering the very strong electron acceptor capability, one of the rational strategies to reduce the absorption, as well as achieve a transparency–nonlinearity balance, is to select oxygen-containing donor groups with moderate electron donating ability. Based on this strategy, MBI with a classical CH_3O- electron-donor (Figure 14 and Table 4) was recently designed. MBI successfully exhibits a maximum absorption wavelength of 443 nm in methanol, which is blue-shifted compared with DAST (λ_{max} = 475 nm) but still exceeds the OH1 benchmark crystal (λ_{max} = 426 nm).

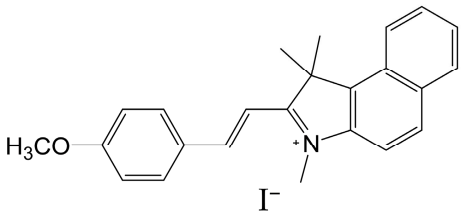

Figure 14. Chemical structure of benzoindolium-based MBI.

Table 4. Comparison of the mentioned indolium-based, benzoindolium-based, and benzimidazolium-based THz crystals.

Crystal Name	Space Group	λ_{max}(nm) in Methanol	β_{max} (Cation)	SHG Intensity	Ref.
EHPSI-4NBS	Monoclinic *Pn*	549	123 × 10^{-30} esu	-	[52]
OHI-T	Monoclinic *Pn* (m)	437	-	~0.7 × OH1 at 2090 nm	[53]
MBI	Monoclinic *Cc* (m)	443	-	~0.8 × OH1 at 2090 nm	[55]
HMI-TMS	Monoclinic *Pn*	364	~76 × 10^{-30} esu	0.06–0.12 × DAST at 1300–1800 nm	[56]

2.5.2. Effect of the Iodide Anion on the Spatial Arrangement

A structural packing diagram of the MBI crystal with an I^- anion along the *c*-axis is shown in Figure 15a,b. In the same cation layers, the molecules are arranged in the same direction, with almost in a "head-to-tail" style. The angle between the adjacent cation layers is 72.47°. Based on this spatial arrangement, the SHG intensity reaches 0.8 times OH1 under 2090 nm fundamental light. The short-wave cutoff edge of MBI is 639 nm. Compared with the reference crystal DAST (680 nm), MBI can exhibit a wide transmission region and cover a wide pump wavelength range [55].

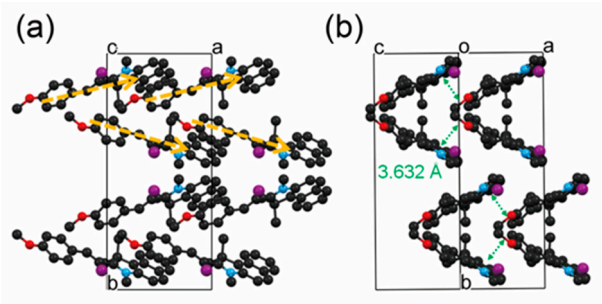

Figure 15. (**a**) Molecule arrangement in the MBI crystal structure along the *c*-axis; (**b**) face-to-face π-π stacking in MBI (3.632 Å) [55].

2.6. Benzimidazolium-Based THz Crystals

2.6.1. Benzimidazolium-Based Cation

As shown in Figure 16, the HMI cation has the same electron donor (HO-, CH_3O-) as quinolinium-based HMQ (Figure 4). The maximum absorption wavelength of HMI-based compounds in methanol is only 364 nm, which is rather small compared with many other ionic-type NLO compounds for THz use [56].

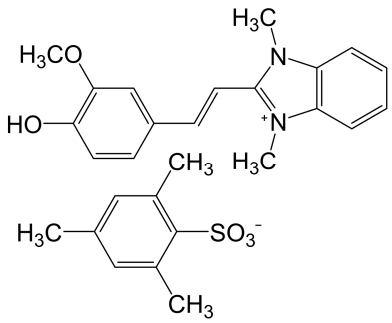

Figure 16. Chemical structure of benzimidazolium-based HMI-TMS.

2.6.2. Anion of HMI-TMS

In an HMI-TMS crystal, with the help of a typical TMS anion, the HMI cations are almost perfectly aligned, maximizing the diagonal component of the second-order nonlinear optical susceptibility. Compared with other series of compounds mentioned above,

HMI-TMS exhibits a wider band gap (~2.95 eV) than OH1 (2.17 eV) [57] and still maintains a large macroscopic optical nonlinearity (the square root of $I_{HMI\text{-}TMS}/I_{DAST}$ is 0.25–0.35 at the fundamental wavelengths from 1300 to 1800 nm). Notably, HMI-TMS results in lower near-infrared refractive index and improved phase matching at around 800 nm [56].

2.7. Crystal Growth

It is of great significance to investigate the crystal growth of high-quality crystals with suitable size and morphology, in order to obtain qualified optical devices. There are different growth methods for organic crystals, such as the solution method, Bridgman–Stockbarger method, and the capillary method [58]. Among them, the solution method is most widely used. Starting with the crystal growth of DAST, extensive studies have been devoted to improving the growth methods and conditions for high-quality crystals. In 1999, a DAST crystal with a size of 5.0 × 4.0 × 0.5 mm^3 was obtained through a slow cooling method, using the "new technology of slope nucleation growth" [59]. In 2008, through the use of constrained spontaneous nucleation and a newly optimized cooling curve, a good optical quality of DAST crystals, with the largest size of 28 × 28 × 8 mm^3, was obtained [60]. Additives have also been considered to improve the morphologies. A DAST crystal with a size of 11 × 8 × 1.2 mm^3 was grown by slow cooling under the control of oleic acid [61]. Recently, DAST crystals were obtained through the seed crystal immobilization method (23 × 22 × 9 mm^3 for high-concentration solutions and 25 × 22 × 2 mm^3 for low-concentration solutions) [62]. Based on crystal growth technology such as DAST, the crystal growth of the mentioned THz crystals, which have been discovered in recent years, can be introduced.

2.7.1. Spontaneous Nucleation Method

Cooling Method

The slow cooling method is one of the most widely used crystal growth technologies for organic crystals. Apart from DAST crystal, newly discovered pyridinium-based NLO crystals, such as OHP-CBS, have also been grown using a slow cooling method in a mixed solvent of methanol and acetonitrile (1:1 mol/mol) at a saturation temperature of 40 °C (Figure 17a), and such a large growth surface of bulk OHP-CBS crystal is sufficient for an optical device [63]. For quinolinium-based THz crystals, the slow cooling method has also been proven as an effective method. With suitable growth conditions, the newly developed OHQ-CBS, with a largest area of 45 mm^2, can be obtained in solvent mixtures with methanol and acetonitrile at 40 °C (Figure 17b). In addition, HMQ-4TFS [29] and halogenated HM6FQ-T [43] can also be grown using the slow cooling method in methanol (Figure 17c,d). HMQ-4TFS crystals were grown with a cooling range from 40 to 30 °C. When the first HMQ-4TFS nucleation appeared, the solution remained at the nucleation temperature for several days, and then dropped to room temperature.

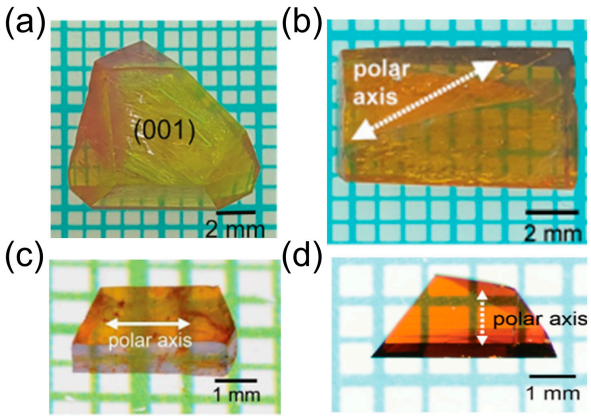

Figure 17. Crystal photos of (**a**) OHP-CBS [63]; (**b**) OHQ-CBS [44]; (**c**) HMQ-4TFS [29]; and (**d**) HM6FQ-T [43].

Benzothiazolium-based PMB-T crystal plate with a large area of 50 mm^2 (Figure 18a) was also obtained through the slow cooling method in methanol acetonitrile mixed solution (1:1 mol/mol) with a saturation temperature of 40 °C and cooling rate of 0.1 °C/d. In particular, as shown in Figure 18b, benzothiazolium-based OHB-TFO crystal grown by the slow cooling method in ethanol presents a plate shape, which is suitable for most optical experiments [49]. However, the morphology (triangular) of OHB-TFO still needs to be improved, and the square shape of the single crystal is ideal for obtaining a larger aperture size in optical experiments. Regarding indolium-based EHPSI-4NBS (Figure 18c), a large crystal is not easy to produce, due to the influence of the rotation and vibration of the ethyl group, and the size of the obtained EHPSI-4NBS is 5 × 2 × 0.38 mm^3 [52].

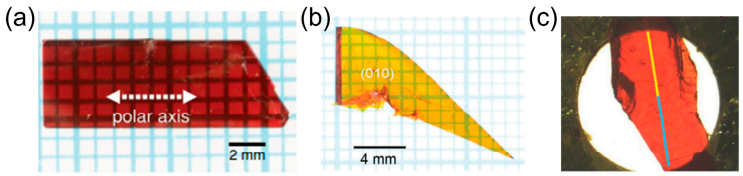

Figure 18. Crystal photos of (**a**) PMB-T [46]; (**b**) OHB-TFO [49]; (**c**) EHPSI-4NBS [52].

Slow Evaporation Method

The slow evaporation method is a classical technique for obtaining crystals; however, a suitable evaporation condition is not very easy to achieve for large-sized crystals with high quality, and not many qualified crystals have been obtained by this method. Plate-like benzothiazolium-based PMB-4TFS was grown though slow evaporation in a methanol and acetonitrile mixed solution (1:1 mol/mol), and the crystal area of PMB-4TFS amounted to 10 mm^2 (Figure 19a) [27]. To choose a suitable solvent to grow benzothiazolium-based HDB-T single crystals with large sizes, the solubility curves of HDB-T in a single methanol and methanol acetonitrile mixed solution (1:1 mol/mol) were measured [48]. HDB-T has a higher solubility in a mixed solvent, and the crystal morphology is suitable, with the size of HDB-T reaching 3 × 2 × 0.8 mm^3 (Figure 19b). Another indolium-based OHI-T (Figure 19c) crystal can be grown by slow evaporation at room temperature and the crystal size can reach 7 × 4 × 1 mm^3, with a rocking curve of 144 arcsec, indicating high quality [53].

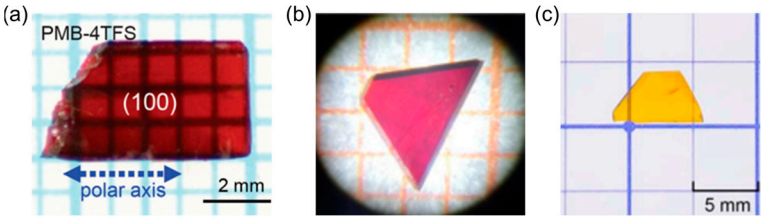

Figure 19. Crystal photos of (**a**) PMB-4TFS [27], (**b**) HDB-T [48], and (**c**) OHI-T [53] grown using slow evaporation.

2.7.2. Seed Method

To grow large-sized crystals, the seed method is commonly used, which is represented by DAST. In this method, not only the solubilities of compounds, but also the quality of the seeds is very important. Benzothiazolium-based HMB-TMS crystals grown using the cooling method at 50 °C can be directly used in optical experiments without optical polishing, through simple cleaving (Figure 20a). The suitable growth range of MBI is 50–45 °C in methanol solution, and MBI crystal was grown using the seed method with a largest size of 10 × 8 × 6 mm^3 (Figure 20b). The rocking curve of a 0.8 mm-thick MBI (*b*-plate) crystal was measured, and the FWHM was 44 arcsec, indicating a good optical quality and sufficient for optical measurement.

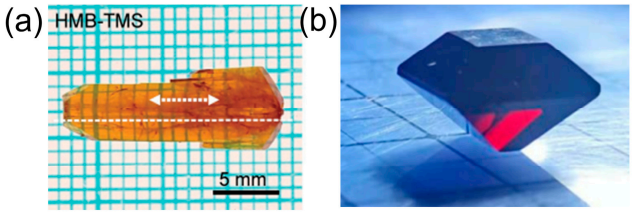

Figure 20. Crystal photos of (**a**) HMB-TMS [47], and (**b**) MBI [55].

2.8. THz Wave Generation

THz radiation generation technology via NLO crystals mainly includes optical rectification (OR) and difference frequency generation (DFG) [64,65]. In recent years, the newly developed crystals have exhibited different absorption characteristics in the working region through rational design of substitution.

2.8.1. Optical Rectification (OR)

Figure 21a shows a THz electric field produced by a 0.31 mm thick OHP-TFS crystal, with a THz output range of 1.5–15 THz (Figure 21b). With the help of strong hydrogen bonds, the absorption coefficient of OHP-TFS crystal shows a lower absorption peak than DAST in the 0.1–4 THz region [28]. Moreover, DHP-TFS with two traditional electron donor HO- groups shows small overall absorption peaks, and a 0.15 mm-thick DHP-TFS crystal produces 20 times the THz amplitude of a 1.0 mm-thick ZnTe crystal (Figure 21c) and a wide THz output range, with the upper cut-off edge being up to 16 THz (Figure 21d) [33].

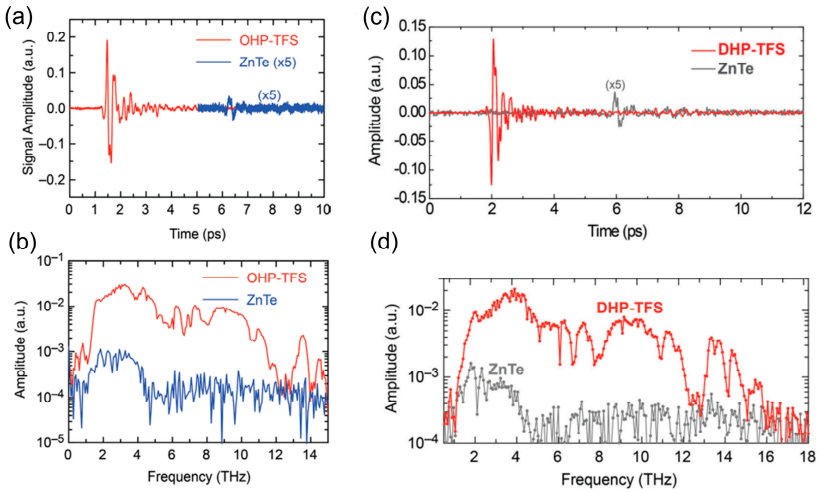

Figure 21. (**a**) Time and (**b**) frequency-domain amplitudes of the THz waves generated in a 0.31 mm thick OHP-TFS [28]; (**c**) time and (**d**) frequency-domain amplitudes of the THz waves generated in a 0.15 mm-thick DHP-TFS at a 1560 nm wavelength [33].

The peak-to-peak THz amplitudes of HM7ClQ-CBS (0.16 mm) and HM7ClQ-T (0.07 mm) are, respectively, 22 and 15 times ZnTe (1.0 mm), and the upper cut-off frequency is 8 THz (Figure 22) [42]. As the crystal structures of HM7ClQ-CBS and HM7ClQ-T are isomorphic, their THz absorption peak positions and THz spectral characteristics are similar. Unlike DAST crystal, HM7ClQ-CBS and HM7ClQ-T have no strong absorption near 1 THz for the formation of more hydrogen bonds. Similarly, OHQ-CBS also shows a rather weak absorption at 1.1 and 1.6 THz [44].

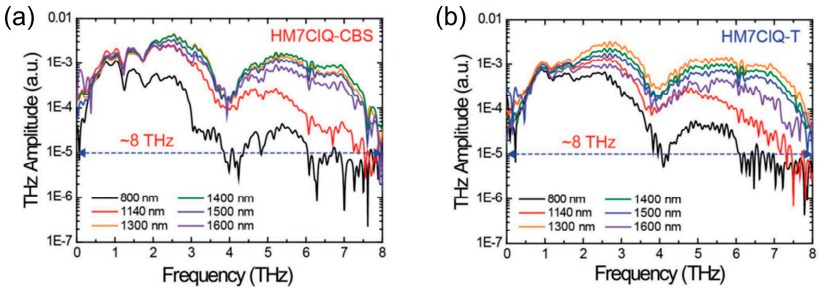

Figure 22. THz amplitude spectra generated in (**a**) 0.16 mm thick HM7ClQ-CBS and (**b**) 0.07 mm thick HM7ClQ-T crystals at different pump wavelengths [42].

The 0.33 mm thick benzothiazolium-based PMB-T terahertz amplitude can reach 430 KVcm^{-1} at a 1300 nm wavelength, higher than a 0.26 mm thick HMB-TMS at the pump pulse energy of 240 µJ (Figure 23a,b). PMB-4TFS (Figure 11a) crystals exhibit a similar upper cut-off frequency to PMB-T, and the introduction of a strong electronegative TFS anion leads to a strongest terahertz output near 1 THz, which is different from the strong absorption near 1 THz of DAST. Moreover, indolium-based EHPSI-4NBS achieved a THz output in the range of 0.1–3.8 THz through optical rectification; and benzoindolium-based crystals P-BI initially achieved a THz output in the range of 0.1–6 THz, of which the maximum output was 2–3 THz (Figure 23c) [54].

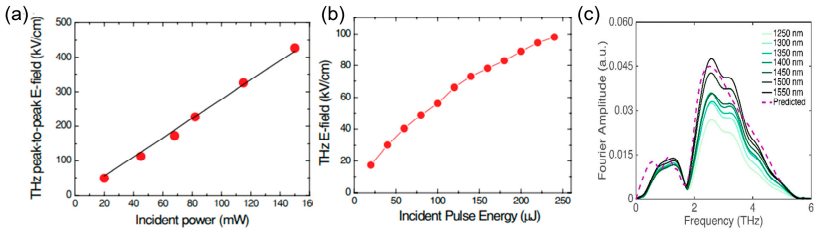

Figure 23. Peak THz E-field generated as a function of incident pulse energy by (**a**) 0.33 mm thick PMB-T [46], (**b**) 0.26 mm thick HMB-TMS [47], and (**c**) THz generation spectrum of P-BI [54].

2.8.2. Difference Frequency Generation (DFG)

Difference frequency generation is an effective way to realize tunable terahertz radiation. Through this method, DAST has achieved an ultra-wide tunable THz output, ranging from 0.1 to 20 THz, with a highest output energy of 870.4 nJ/pulse [62]. In addition, using DFG, the recently developed benzothiazolium-based HDB-T crystal has successfully achieved a tunable THz radiation from 0.1 to 20 THz, and the highest output signal can reach 27 mV at 12.3 THz (Figure 24a), showing superiority in 10 to 14 THz [48]. The OHI-T has also realized an ultra-wide tunable THz output of 0.1–20 THz, as displayed in Figure 24b. In the range of 2.5–15 THz, OHI-T has a better output performance than the OH1 crystal (1.32 mm thickness), and the maximum output energy can reach 25.3 nJ/pulse at 11 THz [53]. A newly discovered benzoindolium-based MBI crystal with classical CH_3O- electron donor, initially achieved an ultra-wide ranged THz output of 2–18 THz under 1.37–1.50 µm dual wavelength laser pumping [55]. Compared with OH1, the THz output of MBI in the range of 11–18 THz may be more advantageous and the pulse energy achieved a 446 nJ/pulse, with the highest conversion efficiency of 4.96×10^{-5} at 12.3 THz (Figure 24c). It should be mentioned that better THz output performance can be expected by improving the quality of these newly discovered crystals and optimizing the pump wavelength and other experimental parameters.

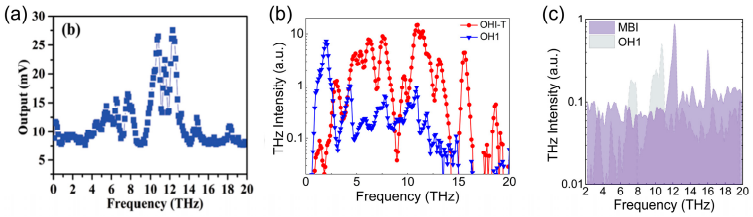

Figure 24. Tuning the THz generation of (**a**) HDB-T [48]; (**b**) OHI-T [53]; and (**c**) 0.8 mm-thick MBI and 0.16 mm-thick OH1 [55].

3. Conclusions

In this work, the recent development of cations and anions in different series of ionic organic NLO crystals was briefly summarized. By the control of the secondary bonds through rational substitution design, various excellent organic nonlinear optical crystals for efficient terahertz-wave radiation have been discovered. The combination of cation and anion substitutions with different electronegativity can effectively contribute to suppressing the molecular vibration in the crystal state, resulting in an improved output spectrum. However, the practical use of these novel materials has been limited so far, and more works on their precise physical properties, such as linear and nonlinear coefficients, are urgently needed, to estimate their application prospects. In addition, it is still a great challenge to find suitable crystal growth conditions for large-sized crystals with a high quality, which is a prerequisite for commercialization. Therefore, more efforts should be devoted to the exploration of novel NLO crystal composition, structure–property relationships, as well as crystal growth techniques, to promote the motif design efficiency and practical application of organic NLO crystals for high-power THz radiation.

Supplementary Materials: The following supporting information can be downloaded at: https://www.mdpi.com/article/10.3390/cryst13010144/s1.

Author Contributions: The manuscript was written through contributions of all authors. All authors have read and agreed to the published version of the manuscript.

Funding: This work was supported by the National Natural Science Foundation of China (Grant No. 52272007, 51902224, 51890864, 51890865).

Institutional Review Board Statement: Not applicable.

Informed Consent Statement: Not applicable.

Data Availability Statement: Not applicable.

Conflicts of Interest: The authors declare no conflict of interest.

References

1. Gao, M.; Zhang, J.; Zhang, X.; Xu, D.; Hu, Z.; Yao, J.; Wu, Y. Steric Group Design for Enhancement of Optical Nonlinearity in Isoxazolone-Based Crystals and Terahertz-Wave Generation. *Cryst. Growth Des.* **2021**, *21*, 3153–3157. [CrossRef]
2. Kim, S.-J.; Kim, S.-I.; Jazbinsek, M.; Yoon, W.; Yun, H.; Kim, D.; Yu, I.C.; Rotermund, F.; Kwon, O.P. Design Strategy of Highly Efficient Nonlinear Optical Orange-Colored Crystals with Two Electron-Withdrawing Groups. *Adv. Photonics Res.* **2022**, *3*, 2100350. [CrossRef]
3. Yu, Z.; Wang, T.; Wang, G.; Xu, K.; Cui, Q.; Cao, L.; Teng, B. Synthesis, growth, structure analysis and performance characterization of DOST crystal: A nonlinear functional material with a wide range of applications. *CrystEngComm* **2020**, *22*, 8362–8373. [CrossRef]
4. Jazbinsek, M.; Puc, U.; Abina, A.; Zidansek, A. Organic Crystals for THz Photonics. *Appl. Sci.* **2019**, *9*, 882. [CrossRef]
5. Sinko, A.; Ozheredov, I.; Rudneva, E.; Manomenova, V.; Kozlova, N.; Lobova, N.; Voloshin, A.; Coutaz, J.-L.; Shkurinov, A. Perspective on Terahertz Applications of Molecular Crystals. *Electronics* **2022**, *11*, 2731. [CrossRef]
6. Chen, J.; Chen, H.; Xu, F.; Cao, L.; Jiang, X.; Yang, S.; Sun, Y.; Zhao, X.; Lin, C.; Ye, N. $Mg_2In_3Si_2P_7$: A Quaternary Diamond-like Phosphide Infrared Nonlinear Optical Material Derived from $ZnGeP_2$. *J. Am. Chem. Soc.* **2021**, *143*, 10309–10316. [CrossRef]
7. Lu, W.; Gao, Z.; Liu, X.; Tian, X.; Wu, Q.; Li, C.; Sun, Y.; Liu, Y.; Tao, X. Rational Design of a $LiNbO_3$-like Nonlinear Optical Crystal, Li_2ZrTeO_6, with High Laser-Damage Threshold and Wide Mid-IR Transparency Window. *J. Am. Chem. Soc.* **2018**, *140*, 13089–13096. [CrossRef]

8. Liao, F.; Wang, Y.; Peng, T.; Peng, J.; Gu, Z.; Yu, H.; Chen, T.; Yu, J.; Gu, F. Highly Efficient Nonlinear Optical Conversion in Waveguiding GaSe Nanoribbons with Pump Pulses Down to a Femto-Joule Level. *Adv. Opt. Mater.* **2018**, *6*, 1701012. [CrossRef]
9. Sun, H.; Liu, J.; Zhou, C.; Yang, W.; Liu, H.; Zhang, X.; Li, Z.; Zhang, B.; Jie, W.; Xu, Y. Enhanced Transmission from Visible to Terahertz in ZnTe Crystals with Scalable Subwavelength Structures. *ACS Appl. Mater. Interfaces* **2021**, *13*, 16997–17005. [CrossRef]
10. Chen, Y.; Hu, C.L.; Fang, Z.; Mao, J.G. $K_2Pb(H_2C_3N_3O_3)(4)(H_2O)(4)$: A potential UV nonlinear optical material with large birefringence. *Inorg. Chem. Front.* **2021**, *8*, 3547–3555. [CrossRef]
11. Guo, J.; Tudi, A.; Han, S.; Yang, Z.; Pan, S. α-SnF_2: A UV Birefringent Material with Large Birefringence and Easy Crystal Growth. *Angew. Chem. Int. Ed. Engl.* **2021**, *60*, 3540–3544. [CrossRef] [PubMed]
12. Wang, W.K.; Mei, D.J.; Liang, F.; Zhao, J.; Wu, Y.D.; Lin, Z.S. Inherent laws between tetrahedral arrangement pattern and optical performance in tetrahedron-based mid-infrared nonlinear optical materials. *Coord. Chem. Rev.* **2020**, *421*, 213444. [CrossRef]
13. Li, Y.; Yin, C.; Yang, X.; Kuang, X.; Chen, J.; He, L.; Ding, Q.; Zhao, S.; Hong, M.; Luo, J. A Nonlinear Optical Switchable Sulfate of Ultrawide Bandgap. *CCS Chem.* **2021**, *3*, 2298–2306. [CrossRef]
14. Liu, Y.; Liu, Y.; Lin, Z.; Li, Y.; Ding, Q.; Chen, X.; Li, L.; Zhao, S.; Hong, M.; Luo, J. Nonpolar $Na_{10}Cd(NO_3)_4(SO_3S)_4$ Exhibits a Large Second-Harmonic Generation. *CCS Chem.* **2022**, *4*, 526–531. [CrossRef]
15. Ma, X.F.; Wang, C.; Zhang, J.; Wang, T.; Wang, A.Y.; Wang, S.Y.; Jia, Z.T.; Zhang, B.T.; He, J.L.; van Smaalen, S.; et al. Broadband BiOCl Nonlinear Saturable Absorber for Watt-Level Passively Q-Switched Yb:LuAG Single Crystal Fiber Laser. *Adv. Opt. Mater.* **2022**, *10*, 2201087. [CrossRef]
16. Liu, X.; Yang, Z.; Wang, D.; Cao, H. Molecular Structures and Second-Order Nonlinear Optical Properties of Ionic Organic Crystal Materials. *Crystals* **2016**, *6*, 158. [CrossRef]
17. Li, B.; He, W.; Wang, L.; Xiao, X.; Yang, H. Effect of lateral fluoro substituents of rodlike tolanecyano mesogens on blue phase temperature ranges. *Soft Matter* **2013**, *9*, 1172–1177. [CrossRef]
18. Rezzonico, D.; Kwon, S.J.; Figi, H.; Kwon, O.P.; Jazbinsek, M.; Gunter, P. Photochemical stability of nonlinear optical chromophores in polymeric and crystalline materials. *J. Chem. Phys.* **2008**, *128*, 124713. [CrossRef]
19. Liu, J.; You, F.; Hu, C.; Ma, Y.; Teng, F.; Wang, T.; Tang, J.; Cao, L.; Teng, B. Growth and characterization of organic 4-chlorobenzaldehyde-N- methyl 4-stilbazolium tosylate crystal: A promising material for nonlinear optical device applications. *Optik* **2019**, *178*, 999–1009. [CrossRef]
20. Pan, F.; Knöpfle, G.; Bosshard, C.; Follonier, S.; Spreiter, R.; Wong, M.S.; Günter, P. Electro-optic properties of the organic salt 4-N,N-dimethylamino-4′-N′-methyl-stilbazolium tosylate. *Appl. Phys. Lett.* **1996**, *69*, 13–15. [CrossRef]
21. Sun, Z.; Liu, X.; Wang, X.; Li, L.; Shi, X.; Li, S.; Ji, C.; Luo, J.; Hong, M. Engineering of Acentric Stilbazolium Salts with Large Second-Order Optical Nonlinearity and Enhanced Environmental Stability. *Cryst. Growth Des.* **2012**, *12*, 6181–6187. [CrossRef]
22. Taniuchi, T.; Ikeda, S.; Mineno, Y.; Okada, S.; Nakanishi, H. Terahertz Properties of a New Organic Crystal, 4′-Dimethylamino-N-methyl-4-stilbazoliump-Chlorobenzenesulfonate. *Jpn. J. Appl. Phys.* **2005**, *44*, L932–L934. [CrossRef]
23. Matsukawa, T.; Notake, T.; Nawata, K.; Inada, S.; Okada, S.; Minamide, H. Terahertz-wave generation from 4-dimethylamino-N′-methyl-4′-stilbazolium p-bromobenzenesulfonate crystal: Effect of halogen substitution in a counter benzenesulfonate of stilbazolium derivatives. *Opt. Mater.* **2014**, *36*, 1995–1999. [CrossRef]
24. Matsukawa, T.; Yoshimura, M.; Takahashi, Y.; Takemoto, Y.; Takeya, K.; Kawayama, I.; Okada, S.; Tonouchi, M.; Kitaoka, Y.; Mori, Y.; et al. Bulk Crystal Growth of Stilbazolium Derivatives for Terahertz Waves Generation. *Jpn. J. Appl. Phys.* **2010**, *49*, 075502. [CrossRef]
25. Wang, T.; Xu, K.; Wang, G.; Wang, Q.; Chen, R.; Ma, J.; Cao, L.; Teng, B. Growth, THz properties, and Hirshfeld surface studies of 4-N,N-dimethylamino-4-N-methyl-stilbazolium 2,4,6-trimethylbenzenesulfonate single crystal. *J. Mater. Sci. Mater. El.* **2022**, *33*, 4704–4711. [CrossRef]
26. Matsukawa, T.; Mineno, Y.; Odani, T.; Okada, S.; Taniuchi, T.; Nakanishi, H. Synthesis and terahertz-wave generation of mixed crystals composed of 1-methyl-4-{2-[4-(dimethylamino)phenyl]ethenyl}pyridinium p-toluenesulfonate and p-chlorobenzenesulfonate. *J. Cryst. Growth* **2007**, *299*, 344–348. [CrossRef]
27. Kim, D.; Kim, W.T.; Seok, J.-H.; Yu, I.C.; Jazbinsek, M.; Yoon, W.; Yun, H.; Kim, D.; Rotermund, F.; Kwon, O.P. Molecular salt crystals with bis(head-to-tail) interionic complementary assembly for efficient organic THz generators. *J. Mater. Chem. C* **2020**, *8*, 10078–10085. [CrossRef]
28. Seok, J.H.; Puc, U.; Kim, S.J.; Yoon, W.; Yun, H.; Yu, I.C.; Rotermund, F.; Kim, D.; Jazbinsek, M.; Kwon, O.P. High-Density Organic Electro-Optic Crystals for Ultra-Broadband THz Spectroscopy. *Adv. Opt. Mater.* **2021**, *9*, 2100618. [CrossRef]
29. Lee, S.-H.; Kang, B.J.; Yoo, B.-W.; Lee, S.-C.; Lee, S.-J.; Jazbinsek, M.; Yun, H.; Rotermund, F.; Kwon, O.P. Terahertz Phonon Mode Engineering of Highly Efficient Organic Terahertz Generators. *Adv. Funct. Mater.* **2017**, *27*, 1605583. [CrossRef]
30. Marder, S.R.; Perry, J.W.; Schaefer, W.P. Synthesis of organic salts with large second-order optical nonlinearities. *Science* **1989**, *245*, 626–628. [CrossRef]
31. Walther, M.; Jensby, K.; Keiding, S.R. Far-infrared properties of DAST. *Opt. Lett.* **2000**, *25*, 911–913. [CrossRef]
32. Zhang, X.; Yan, C.; Xu, D.; Li, Y.; Shi, W.; Zhang, G.; Zhang, X.; Yao, J.; Wu, Y. Widely tunable and monochromatic terahertz difference frequency generation with organic crystal 2-(3-(4-hydroxystyryl)-5,5-dime-thylcyclohex-2-enylidene) malononitrile. *Appl. Phys. Lett.* **2016**, *108*, 011104. [CrossRef]

33. Yoon, G.E.; Seok, J.H.; Puc, U.; Shin, B.R.; Yoon, W.; Yun, H.; Kim, D.; Yu, I.C.; Rotermund, F.; Jazbinsek, M.; et al. Phonon-Suppressing Intermolecular Adhesives: Catechol-Based Broadband Organic THz Generators. *Adv. Sci.* **2022**, *9*, e2201391. [CrossRef] [PubMed]
34. Kim, P.J.; Jeong, J.H.; Jazbinsek, M.; Kwon, S.J.; Yun, H.; Kim, J.T.; Lee, Y.S.; Baek, I.H.; Rotermund, F.; Günter, P.; et al. Acentric nonlinear optical N-benzyl stilbazolium crystals with high environmental stability and enhanced molecular nonlinearity in solid state. *CrystEngComm* **2011**, *13*, 444–451. [CrossRef]
35. Lee, S.C.; Kang, B.J.; Koo, M.J.; Lee, S.H.; Han, J.H.; Choi, J.Y.; Kim, W.T.; Jazbinsek, M.; Yun, H.; Kim, D.; et al. New Electro-Optic Salt Crystals for Efficient Terahertz Wave Generation by Direct Pumping at Ti:Sapphire Wavelength. *Adv. Opt. Mater.* **2017**, *5*, 1600758. [CrossRef]
36. Kang, B.J.; Baek, I.H.; Jeong, J.-H.; Kim, J.-S.; Lee, S.-H.; Kwon, O.P.; Rotermund, F. Characteristics of efficient few-cycle terahertz radiation generated in as-grown nonlinear organic single crystals. *Curr. Appl. Phys.* **2014**, *14*, 403–406. [CrossRef]
37. Jeong, J.H.; Kang, B.J.; Kim, J.S.; Jazbinsek, M.; Lee, S.H.; Lee, S.C.; Baek, I.H.; Yun, H.; Kim, J.; Lee, Y.S.; et al. High-power broadband organic THz generator. *Sci. Rep.* **2013**, *3*, 3200. [CrossRef] [PubMed]
38. Kim, P.J.; Jeong, J.H.; Jazbinsek, M.; Choi, S.B.; Baek, I.H.; Kim, J.T.; Rotermund, F.; Yun, H.; Lee, Y.S.; Günter, P.; et al. Highly Efficient Organic THz Generator Pumped at Near-Infrared: Quinolinium Single Crystals. *Adv. Funct. Mater.* **2012**, *22*, 200–209. [CrossRef]
39. Kwon, O.P.; Kwon, S.J.; Jazbinsek, M.; Brunner, F.D.J.; Seo, J.I.; Hunziker, C.; Schneider, A.; Yun, H.; Lee, Y.S.; Günter, P. Organic Phenolic Configurationally Locked Polyene Single Crystals for Electro-optic and Terahertz Wave Applications. *Adv. Funct. Mater.* **2008**, *18*, 3242–3250. [CrossRef]
40. Lee, S.H.; Kang, B.J.; Kim, J.S.; Yoo, B.W.; Jeong, J.H.; Lee, K.H.; Jazbinsek, M.; Kim, J.W.; Yun, H.; Kim, J.; et al. New Acentric Core Structure for Organic Electrooptic Crystals Optimal for Efficient Optical-to-THz Conversion. *Adv. Opt. Mater.* **2015**, *3*, 756–762. [CrossRef]
41. Gilday, L.C.; Robinson, S.W.; Barendt, T.A.; Langton, M.J.; Mullaney, B.R.; Beer, P.D. Halogen Bonding in Supramolecular Chemistry. *Chem. Rev.* **2015**, *115*, 7118–7195. [CrossRef] [PubMed]
42. Kim, S.I.; Kim, W.T.; Seok, J.H.; Jazbinsek, M.; Yoon, W.; Yu, I.C.; Yun, H.; Kim, D.; Rotermund, F.; Kwon, O.P. Organic σ-Hole Containing Crystals with Enhanced Nonlinear Optical Response and Efficient Optical-to-THz Frequency Conversion. *Adv. Opt. Mater.* **2020**, *8*, 1901840. [CrossRef]
43. Kim, S.-I.; Kang, B.J.; Jeong, C.-U.; Shin, M.-H.; Kim, W.T.; Jazbinsek, M.; Yoon, W.; Yun, H.; Kim, D.; Rotermund, F.; et al. Fluorinated Organic Electro-Optic Quinolinium Crystals for THz Wave Generation. *Adv. Opt. Mater.* **2019**, *7*, 1801495. [CrossRef]
44. Lee, S.-J.; Kang, B.J.; Shin, M.-H.; Lee, S.-C.; Lee, S.-H.; Jazbinsek, M.; Yun, H.; Kim, D.; Rotermund, F.; Kwon, O.P. Efficient Optical-to-THz Conversion Organic Crystals with Simultaneous Electron Withdrawing and Donating Halogen Substituents. *Adv. Opt. Mater.* **2018**, *6*, 1700930. [CrossRef]
45. Shin, M.H.; Kim, W.T.; Kim, S.I.; Lee, S.H.; Yu, I.C.; Jazbinsek, M.; Yoon, W.; Yun, H.; Kim, D.; Rotermund, F.; et al. Efficient Gap-Free Broadband Terahertz Generators Based on New Organic Quinolinium Single Crystals. *Adv. Opt. Mater.* **2019**, *7*, 1900953. [CrossRef]
46. Lee, S.C.; Kang, B.J.; Lee, J.A.; Lee, S.H.; Jazbinsek, M.; Yoon, W.; Yun, H.; Rotermund, F.; Kwon, O.P. Single Crystals Based on Hydrogen-Bonding Mediated Cation-Anion Assembly with Extremely Large Optical Nonlinearity and Their Application for Intense THz Wave Generation. *Adv. Opt. Mater.* **2018**, *6*, 1701258. [CrossRef]
47. Lee, S.H.; Lu, J.; Lee, S.J.; Han, J.H.; Jeong, C.U.; Lee, S.C.; Li, X.; Jazbinsek, M.; Yoon, W.; Yun, H.; et al. Benzothiazolium Single Crystals: A New Class of Nonlinear Optical Crystals with Efficient THz Wave Generation. *Adv. Mater.* **2017**, *29*, 1701748. [CrossRef] [PubMed]
48. Shi, J.; Liang, F.; He, Y.; Zhang, X.; Lin, Z.; Xu, D.; Hu, Z.; Yao, J.; Wu, Y. Rational structural design of benzothiazolium-based crystal HDB-T with high nonlinearity and efficient terahertz-wave generation. *Chem. Commun.* **2019**, *55*, 7950–7953. [CrossRef]
49. Shin, M.H.; Kim, W.T.; Kim, S.I.; Kim, S.J.; Yu, I.C.; Kim, S.W.; Jazbinsek, M.; Yoon, W.; Yun, H.; Rotermund, F.; et al. Organic Broadband THz Generators Optimized for Efficient Near-Infrared Optical Pumping. *Adv. Sci.* **2020**, *7*, 2001738. [CrossRef]
50. Lee, J.A.; Kim, W.T.; Jazbinsek, M.; Kim, D.; Lee, S.H.; Yu, I.C.; Yoon, W.; Yun, H.; Rotermund, F.; Kwon, O.P. X-Shaped Alignment of Chromophores: Potential Alternative for Efficient Organic Terahertz Generators. *Adv. Opt. Mater.* **2020**, *8*, 1901921. [CrossRef]
51. Kim, S.-J.; Yu, I.C.; Lee, J.-A.; Kim, W.T.; Jazbinsek, M.; Yoon, W.; Yun, H.; Rotermund, F.; Kwon, O.P. New benzothiazolium crystals with very large off-diagonal optical nonlinearity. *Dye. Pigment.* **2021**, *192*, 109433. [CrossRef]
52. Valdivia-Berroeta, G.A.; Jackson, E.W.; Kenney, K.C.; Wayment, A.X.; Tangen, I.C.; Bahr, C.B.; Smith, S.J.; Michaelis, D.J.; Johnson, J.A. Designing Non-Centrosymmetric Molecular Crystals: Optimal Packing May Be Just One Carbon Away. *Adv. Funct. Mater.* **2019**, *30*, 1904786. [CrossRef]
53. Shi, J.; He, Y.; Liang, F.; Zhang, X.; Xu, D.; Yao, J.; Zhang, G.; Hu, Z.; Yao, J.; Wu, Y. Methyl substitution for noncentrosymmetric stacking: A promising organic single crystal for highly efficient terahertz-wave generation. *J. Mater. Chem. C* **2020**, *8*, 4226–4233. [CrossRef]
54. Valdivia-Berroeta, G.A.; Heki, L.K.; Jackson, E.W.; Tangen, I.C.; Bahr, C.B.; Smith, S.J.; Michaelis, D.J.; Johnson, J.A. Terahertz generation and optical characteristics of P-BI. *Opt. Lett.* **2019**, *44*, 4279–4282. [CrossRef]

55. Zhang, W.F.; Wang, Z.L.; Zhang, X.Y.; Wang, Y.Y.; Xu, D.G.; Hu, Z.G.; Yao, J.Q.; Wu, Y.C. Nonlinear Optical Benzoindolium-Based Single Crystals: H-Contacts Induced Noncentrosymmetric Alignment Approaching Efficient Terahertz-Wave Generation. *Cryst. Growth Des.* **2022**, *22*, 3311–3318. [CrossRef]
56. Kim, D.; Kim, W.T.; Han, J.H.; Lee, J.A.; Lee, S.H.; Kang, B.J.; Jazbinsek, M.; Yoon, W.; Yun, H.; Kim, D.; et al. Wide-Bandgap Organic Crystals: Enhanced Optical-to-Terahertz Nonlinear Frequency Conversion at Near-Infrared Pumping. *Adv. Opt. Mater.* **2020**, *8*, 1902099. [CrossRef]
57. Bharath, D.; Kalainathan, S. Dielectric, optical and mechanical studies of phenolic polyene OH1 organic electrooptic crystal. *Opt. Laser Technol.* **2014**, *63*, 90–97. [CrossRef]
58. Yokoo, A.; Yokohama, I.; Takara, H.; Kaino, T. Growth method, optical properties, and application of organic nonlinear optical crystal 2-adamantylamino-5-nitropyridine. In Proceedings of the Nonlinear Optical Properties of Organic Materials X, San Diego, CA, USA, 30 July–1 August 1997.
59. Adachi, H.; Takahashi, Y.; Yabuzaki, J.; Mori, Y.; Sasaki, T. Growth of high quality nonlinear optical crystal 4-dimethylamino-N-methyl-4-stilbazolium tosylate (DAST). *J. Cryst. Growth* **1999**, *198*, 568–571. [CrossRef]
60. Ruiz, B.; Jazbinsek, M.; Günter, P. Crystal Growth of DAST. *Cryst. Growth Des.* **2008**, *8*, 4173–4184. [CrossRef]
61. Wen, X.; Xu, X.; Zhou, H.; Hu, L.; Jing, Y.; Xu, J.; Cheng, X.; Shi, J.; Liu, X.; Fan, T.; et al. Growth of 4-N,N-Dimethylamino-4′-N′-methyl-stilbazolium Tosylate (DAST) Organic Single Crystals Controlled by Oleic Acid. *Crystals* **2019**, *9*, 494. [CrossRef]
62. You, F.; Wang, T.; Wang, Q.; Cao, L.; Zhong, D.; Ji, S.; Hao, L.; Teng, B.; Tang, J. Stable growth of large-size organic 4-N,N-dimethylamino-4′-N′-methyl-stilbazolium tosylate crystal and its optical, dielectric and THz properties. *J. Mol. Struct.* **2021**, *1236*, 130360. [CrossRef]
63. Jeong, C.-U.; Kang, B.J.; Lee, S.-H.; Lee, S.-C.; Kim, W.T.; Jazbinsek, M.; Yoon, W.; Yun, H.; Kim, D.; Rotermund, F.; et al. Yellow-Colored Electro-Optic Crystals as Intense Terahertz Wave Sources. *Adv. Funct. Mater.* **2018**, *28*, 1801143. [CrossRef]
64. Suizu, K.; Miyamoto, K.; Yamashita, T.; Ito, H. High-power terahertz-wave generation using DAST crystal and detection using mid-infrared powermeter. *Opt. Lett.* **2007**, *32*, 2885–2887. [CrossRef] [PubMed]
65. Schneider, A.; Neis, M.; Stillhart, M.; Ruiz, B.; Khan, R.U.A.; Günter, P. Generation of terahertz pulses through optical rectification in organic DAST crystals: Theory and experiment. *J. Opt. Soc. Am. B* **2006**, *23*, 1822–1835. [CrossRef]

Disclaimer/Publisher's Note: The statements, opinions and data contained in all publications are solely those of the individual author(s) and contributor(s) and not of MDPI and/or the editor(s). MDPI and/or the editor(s) disclaim responsibility for any injury to people or property resulting from any ideas, methods, instructions or products referred to in the content.